

# Coherent laminar and turbulent motion of toroidal vortex bundles

D.H. Wacks,<sup>1</sup> A. W. Baggaley,<sup>2</sup> and C. F. Barenghi<sup>3</sup>

<sup>1</sup>*School of Mechanical and Systems Engineering, Newcastle University,  
Newcastle upon Tyne NE1 7RU, United Kingdom*

<sup>2</sup>*School of Mathematics and Statistics, University of Glasgow, Glasgow G12 8QW, Scotland, United Kingdom*

<sup>3</sup>*Joint Quantum Centre (JQC) Durham-Newcastle,  
and School of Mathematics and Statistics, Newcastle University,  
Newcastle upon Tyne, NE1 7RU, United Kingdom*

(Dated: July 29, 2021)

Motivated by experiments performed in superfluid helium, we study numerically the motion of toroidal bundles of vortex filaments in an inviscid fluid. We find that the evolution of these large-scale vortex structures involves the generalised leapfrogging of the constituent vortex rings. Despite three dimensional perturbations in the form of Kelvin waves and vortex reconnections, toroidal vortex bundles retain their coherence over a relatively large distance (compared to their size), in agreement with experimental observations.

## I. INTRODUCTION

This work is motivated by a series of experiments [1–3] performed in the 1980’s in which Borner and collaborators forced superfluid helium ( $^4\text{He}$ ) through the circular orifice of a cylindrical tube (diameter  $D = 0.8$  cm) by the single stroke of a piston, at temperatures between 1.3 and 2.15 K above absolute zero. Using acoustic methods, Borner *et al.* determined size, position, velocity and superfluid circulation of the localised vortex structure which was ejected from the tube’s orifice. Their finding that velocity and circulation remained reproducibly constant during the evolution suggested that the vortex structure maintained its identity and travelled coherently.

To appreciate the significance of Borner’s result, we recall [4] that the flow of superfluid helium is potential (in a quantum fluid, the velocity is proportional to the gradient of the phase of the quantum mechanical wave function). Superfluid vorticity exists only in the form of thin vortex lines of atomic thickness (the radius of the vortex core is  $a \approx 10^{-8}$  cm) and fixed circulation  $\kappa = 9.97 \times 10^{-4}$  cm<sup>2</sup>/s proportional to Planck’s constant. The superfluid literature is familiar [5] with individual vortex rings, ranging in diameter from approximately one micron (for rings generated by a high voltage tip [6]) to half a millimetre (as recently visualized by Bewley and Sreenivasan [7]). However, the circulation  $\Gamma$  observed by Borner was much larger than the quantum of circulation  $\kappa$ : they reported values in the range from  $\Gamma = 2.3$  to 4.85 cm<sup>2</sup>/s depending on piston’s stroke, velocity and temperature. According to Borner, the cylinder-piston arrangement generates a macroscopic, self-propelling, toroidal vortex structure - some kind of large-scale vortex ring. The natural interpretation is that such structure actually consists of a toroidal bundle of  $N = \Gamma/\kappa \approx 10^3$  individual vortex rings of the same polarity travelling in the same direction at close distance from each other, hence interacting strongly but remaining coherent during the observed evolution over a distance of about 6 cm.

Borner’s interpretation was strengthened by further experiments performed by Murakami and collaborators [8]. Using a cylinder-piston arrangement of the same size as Borner’s, Murakami *et al.* succeeded in visualizing Borner’s large-scale vortex ring and tracking its motion by means of frozen hydrogen-deuterium particles trapped in the cores of individual vortex rings. Stamm and collaborators [9, 10] also generated large-scale vortex rings in liquid helium, but using a different technique (second-sound heat pulses), which resulted in vortex structures less stable than Borner’s and Murakami’s.

Unfortunately the experiments of Borner, Murakami and Stamm were not followed up and became almost forgotten. Today the situation has changed. Current experimental, numerical and theoretical work is concerned with similarities between superfluid turbulence and ordinary turbulence. In particular, the energy spectrum [11–15] which is observed in turbulent superfluid helium obeys the same Kolmogorov scaling of ordinary turbulence. It has been argued [16, 17] that this property arises from the partial polarization of superfluid vortex lines. The existence of bundles of vortices in turbulent helium is also debated [18, 19], in analogy with the “worms” which are responsible for the intermittency of ordinary turbulence [20]. Issues raised by Borner’s and Murakami’s experiments, such as the interaction of vortex lines, their polarization, coherence and stability, have thus become important. Moreover, Borner’s cylinder-piston arrangement is a convenient configuration to study polarized vortex lines under controlled experimental conditions.

Thus motivated, we revisit Borner’s and Murakami’s experiments. Our work is not to model the experiments precisely, or to perform linear stability calculations (it is not even clear what should be the state to perturb). We simply want to gain qualitative insight into the three-dimensional motion and stability of a number of coaxial, thin cored vortex rings arranged in the shape of a toroidal bundle, as envisaged by Borner. Will such a vortex configuration travel a significant distance (larger than its diameter) in a coherent way, before becoming unstable, or will vortex interactions destroy the structure straight away?

Borner’s experiment has another interesting fluid dynamics aspect. It is well-known that two coaxial vortex rings of the same polarity, when close to each other, execute a peculiar leapfrogging motion [21–24]: the ring behind shrinks, speeds up, goes inside the ring which was ahead, overtakes it, grows in size, slows down, and then the process repeats in a periodic fashion. For a toroidal bundle of many ( $N \gg 2$ ) vortex rings to remain coherent, some kind of generalized leapfrogging motion is likely to take place.

Before we finish this introduction, we recall [4] the classical expressions for the velocity  $v$  and the energy (per unit density)  $E$  of a vortex ring of radius  $R$ :

$$v = \frac{\Gamma}{4\pi R} (\ln(8R/a) - \alpha), \quad (1)$$

$$E = \frac{1}{2} \Gamma^2 R (\ln(8R/a) - \beta), \quad (2)$$

where  $a$  is the core radius and  $\Gamma$  is the circulation; the quantities  $\alpha$  and  $\beta$  depend on the assumed vortex core structure [4]. For hollow core we have  $\alpha = 1/2$  and  $\beta = 3/2$ ; for core rotating at uniform angular velocity as a solid-body

(Rankine vortex) we have  $\alpha = 1/4$  and  $\beta = 7/4$  [25]. For a single quantum vortex ring, the quantities  $\Gamma$  and  $a$  must be replaced by the quantum of circulation  $\kappa$  and the superfluid vortex core radius  $a_0 = 1.3 \times 10^{-8}$  cm (proportional to the superfluid healing length). For Borner's large-scale vortex ring structure, which we model as a torus,  $R$  will be the major radius of the torus and  $a$  the minor radius.

## II. METHOD

For the sake of simplicity, we ignore the thermal excitations which make up helium's normal fluid [4]. This approximation is justified by the fact that, at the lowest temperature explored by Borner, the normal fluid fraction is only 4.5 percent of the total density [26]. In this low temperature limit, friction is negligible [26] and vortex lines move with the superfluid. We are thus in the limit of classical Euler dynamics. We represent vortex lines as three-dimensional, closed space curves  $\mathbf{s} = \mathbf{s}(\xi, t)$  of infinitesimal thickness and circulation  $\kappa$  moving in an inviscid, incompressible Euler fluid. The curves are parametrised by arc length  $\xi$  and evolve in time  $t$  in an infinite computational domain according to the Biot-Savart law [27]

$$\frac{d\mathbf{s}}{dt} = -\frac{\kappa}{4\pi} \oint_{\mathcal{L}} \frac{(\mathbf{s} - \mathbf{r})}{|\mathbf{s} - \mathbf{r}|^3} \times d\mathbf{r}, \quad (3)$$

where the line integral extends over the entire vortex configuration  $\mathcal{L}$ . Vortex reconnections are forbidden by Euler dynamics, but are possible for quantum vortices [28–30]. Therefore we supplement Eq. 3 with an algorithmic reconnection procedure which changes the topology of the vortex configuration when the distance between two filaments is less than a prescribed cutoff value. In the next sections, when describing results, we shall state explicitly whether vortex reconnections have taken place or not; in this way we shall distinguish the aspects of our problem which refer to classical Eulerian fluid dynamics from the aspects which (since reconnections have taken place) are relevant only to superfluid liquid helium.

The numerical techniques which we use to discretize the vortex lines, compute their evolution and de-singularize the Biot-Savart integral (using the superfluid vortex core radius  $a_0$ ) are described in our previous papers [33, 34]. Here it suffices to recall that the relative distance between discretization points along filaments is held approximately between  $\Delta\xi$  and  $\Delta\xi/2$  where  $\Delta\xi$  represents the prescribed numerical resolution. To make direct comparison with related vortex filament calculations performed by Schwarz [31] and Tsubota & Adachi [32] we run our simulations with vortex core cutoff corresponding to uniformly rotating solid-body core, and find good agreement [18]. The reconnection algorithm, triggered when the vortex separation is closer than  $\Delta\xi/2$ , was described by Baggaley [35] who compared it to other algorithms used in the liquid helium literature. A more microscopic model based on the Gross-Pitaevskii equation for a Bose-Einstein condensate suggests that at each reconnection a small amount of kinetic energy is turned into sound [29, 36]. To account for this effect, at each reconnection the algorithm reduces the total vortex length (used as a proxy for energy), whereas, in the absence of reconnections, according to Eulerian dynamics the energy is conserved during the evolution.

Our model is based on the assumption that, apart from isolated reconnection events, the vortex filaments are usually far from each other compared to the vortex core thickness  $a_0$ . This assumption is justified by the following argument: let  $R$  and  $a$  be respectively the major and minor radius of the toroidal structure generated by the piston in Borner's experiment; using Eq. 1 and the observed values of  $\Gamma$  and  $v$ , we estimate the minor radius of the torus,  $a$ , and find that the typical distance between vortex lines,  $\ell \approx n_0^{-1/2} \approx 0.003$  cm (where  $n_0 = N/(\pi a^2)$  is the number of vortex lines per unit cross section of the torus) is indeed many orders of magnitude bigger than  $a_0$ .

## III. INITIAL CONDITION

We do not have enough experimental information about the formation of Borner's large-scale helium vortex ring as it rolls out of the orifice. Moreover, the vortex filament method is not suitable for describing the process of vortex nucleation - the Gross-Pitaevskii nonlinear Schroedinger Equation should be used instead. Even neglecting the formation process near the orifice, we do not know if there is a steady or periodic vortex configuration which travels away from the orifice, whose linear or nonlinear stability can be studied - perhaps there is not, and the problem is essentially an initial value one. For the sake of simplicity, our initial condition consists of  $N$  coaxial vortex rings lying in the  $yz$ -plane within a torus of major radius  $R$  and minor radius  $a$ , oriented to travel in the  $x$ -direction.. For  $N \geq 7$  the rings are arranged in a hexagonal pattern on the cross section of the torus such that each successive hexagonal layer is at distance  $\ell$  further way from the centre than the previous layer. This configuration is the most energetically

favourable for a vortex lattice in a rotating cylinder, as described by Donnelly [4]. The number of initial vortex rings is thus  $N = 3n(n - 1) + 1 = 7, 19, 37, 61, 91, \dots$  for  $n > 1$  where  $n$  is the layer's number.  $N = 2$  is a special case, as the two rings are at the same time co-axial and concentric, lying on the same  $yz$ -plane at distance  $\ell = 2a$  from each other.  $N = 3$  is another special case: the cross section has the shape of an equilateral triangle and  $a = \ell/\sqrt{3}$ . In general, for  $n \geq 2$ ,  $a = (n - 1)\ell$ . Examples of initial conditions with  $N = 2, 3, 7$  and 19 rings are shown in Fig. 1.

Borner and collaborators measured experimentally the large and small radii of the large-scale rings,  $R$  and  $a$ , as well as the circulation  $\Gamma$ . They reported that  $R \approx 0.4$  cm or slightly larger, consistently with the observation [37, 38] that, in an ordinary fluid, the ring which is generated by the piston-cylinder arrangement is somewhat larger than the orifice, and that  $R/a \approx 4$ . The estimated values of the intervortex distance  $\ell$  vary from approximately  $10^{-2}$  to  $10^{-4}$  cm.

#### IV. COMPUTATIONAL CONSTRAINTS AND TESTS

Our main computational constraint is the evaluation of Biot-Savart integrals, which grows with  $N_p^2$ , where  $N_p$  is the number of discretization points along the vortices.  $N_p$  is determined by the parameter  $\Delta\xi$  (the distance between discretization points) and the total vortex length (which depends on the number  $N$  of vortex rings and their radius). Clearly  $\Delta\xi$  must be smaller than the distance between vortex rings, which depends on  $N$  and  $a$ . Furthermore, to ensure the numerical stability of the evolution, the time step  $\Delta t$  must be small enough to resolve the shortest, fastest-rotating Kelvin waves (helical perturbations along the vortex filaments) which have wavelength of the order of  $\Delta\xi$ . Therefore a decrease of  $\Delta\xi$  requires a decrease of  $\Delta t$ . This means that, whereas the cost of a single time-step scales as  $N_p^2$ , the cost of computing the evolution up to a given time actually scales as  $N_p^3$ .

We do not have the computing power to compute the long-term evolution of vortex bundles with the very large number of vortex rings of Borner's experiments ( $N \sim 10^3$ ), but we shall see that the values of  $N_p$  which we can afford give us qualitative information about the motion of small vortex bundles, and provide us with insight into the conditions of the experiments.

To test the computer code, we verify that a single ( $N = 1$ ) vortex ring travels at constant energy  $E$  with steady translational velocity  $v$ . The velocity is computed from the time to travel a given distance (for  $N > 1$  we track the motion of the centre of vorticity instead). For example, for a single vortex ring of radius  $R = 0.0896$  cm with  $\Delta\xi = 0.00015$  cm, we find that  $v = 0.01573$  cm/s differs from the value predicted by Eq. (1) with the Rankine core model,  $v = 0.01556$  cm/s, by approximately 1%. The energy (per unit density) is computed using the expression

$$E = \frac{1}{2} \int_V \mathbf{v}^2 dV = \kappa \oint_{\mathcal{L}} \mathbf{v} \cdot \mathbf{s} \times \mathbf{s}' d\xi, \quad (4)$$

where we have assumed that the vorticity is concentrated along the vortex filaments and that the velocity goes to zero at infinity. For a single vortex ring, we find that energy is conserved to within  $10^{-12}\%$  for typical time scales and length scales investigated. The case of  $N = 2$  leapfrogging vortex rings is more challenging because energy conservation is tested under the action of a re-meshing algorithm (the number of discretization points on a ring changes as the ring grows and shrinks in size). We find that energy is conserved to within 0.5%. Fig. 2 shows stable leapfrogging of two concentric coaxial rings for a distance of about 40 diameters. The figure also demonstrates that the motion does not depend on the numerical resolution parameter  $\Delta\xi$ . The speed of translation of the vortex bundles is tested by changing the resolution  $\Delta\xi$ . For example, consider the bundle of  $N = 3$  vortex rings with  $R = 0.06$  cm,  $\ell = 0.015$  cm,  $a = \ell/\sqrt{3}$ ,  $R/a = 6.92$ . Using resolution  $\Delta\xi = 0.00149$  cm ( $\ell/\Delta\xi = 10$ ) we find that (with time step  $\Delta t = 5 \times 10^{-5}$  s) it travels the distance  $\Delta x/D = 10.24$  (compared to its initial diameter) in  $t = 40$  s, hence the average speed is  $v = 0.031$  cm/s. If we reduce the resolution to  $\Delta\xi = 0.00125$  cm (with  $\Delta t = 3 \times 10^{-5}$  s) and  $\Delta\xi = 0.00075$  cm (with  $\Delta t = 1.5 \times 10^{-5}$  s) we find that in both cases it reaches  $\Delta x/D = 11.525$  in  $t = 45$  s, which still corresponds to  $v = 0.031$  cm/s.

Finally, we test energy conservation during the evolution of larger vortex bundles ( $N = 3, 7, 19$ ). For the length scales and time scales investigated, we find that the relative error  $(E(t) - E(0))/E(0)$  is always well below 1%, provided that no vortex reconnections have taken place.

## V. RESULTS

### A. Coherent motion of toroidal vortex bundles

We now proceed to investigate the motion of bundles of vortex rings with  $N = 1, 3, 7, 19$ . The parameters of the simulations are shown in Table I. In all runs we set up the initial condition so that  $\ell = 0.015$  cm and  $R = 0.06$  cm. For  $N = 19$ , since  $a = 2\ell$ ,  $R = 0.06$  cm would have meant that  $a = 0.003$  cm, hence  $R/a = 2$ , and the leapfrogging motion, at least in two-dimensions, may not be stable [41]. Therefore, for  $N = 19$  only, we set  $R = 0.12$  cm and  $R/a = 4$ . In all cases we find that the vortex bundles travel at approximately constant speed without disintegrating, and reach the distance  $10D$  (observed by Borner) after approximately 50, 40, 35 and 25 s respectively. Fig. 3 shows the distance travelled,  $\Delta x$ , in units of the initial diameter  $D$  vs time  $t$  for toroidal bundles consisting of  $N = 1, 2, 3, 7$  and 19 vortex rings; it is apparent that all bundles travel at essentially constant velocity (the largest bundle slows down slightly).

Table II gives quantitative information about each simulation: average curvature  $\bar{c}$ , translational velocity  $v$  of centre of vorticity, distance travelled  $\Delta x$  in units of the initial diameter  $D$ , and vortex length  $\Lambda$ . Changes in length and curvature reflect the appearance of Kelvin waves along the filaments. The labels “start”, “finish” and “reconnection” denote the times at which we start and stop a simulation, and the time at which the first vortex reconnection (if any) has taken place. As mentioned in Section II, classical Eulerian dynamics breaks down at the first reconnection; beyond the first reconnection, our results are still valid for superfluid liquid.

### B. Velocity and energy

As explained in Section IV, the available computing power limits our simulations to a number of vortex rings (up to  $N = 19$  in the previous subsection) which is much less than in Borner’s experiment. To bridge this gap, we have performed shorter numerical simulations of only few time steps in order to determine the initial instantaneous velocity of vortex bundles with experimentally realistic values of  $N$ , up to  $N = 1027$ , the first  $O(10^3)$  hexagonally centred number. The limitation of this comparison is that the vortex bundle does not have time to distort its initially circular shape and acquire the slightly elliptical cross section which we observe in long-term simulations. Fig. 4(a) shows that the translational velocity  $v$  determined numerically in this way for large vortex bundles (red circles) is in good agreement with Borner’s experiments (black squares and diamonds).

In the limit  $R \gg a$ , simple models of the translational velocity and energy of a vortex bundle of  $N$  vortex rings is obtained by generalizing Eq. 1 and 2:

$$v' = \frac{N\kappa}{4\pi R} (\ln(8R/a) - \alpha), \quad (5)$$

$$E' = \frac{1}{2} N^2 \kappa^2 R (\ln(8R/a) - \beta), \quad (6)$$

where  $a$  is now the minor radius of the torus and  $N\kappa$  has replaced  $\kappa$ . The blue line in Fig. 4(a,b), calculated for the hollow core model, shows that this model is indeed a good approximation.

### C. Generalized leapfrogging

The coherent motion of the vortex bundles which we obtain (before instabilities and reconnections occur) results from a generalised form of the familiar, ordinary leapfrogging of  $N = 2$  vortex rings. As the toroidal vortex structure moves along its axis, the individual vortex rings at the back of the torus shrink and slip through the middle, speeding up their translational velocity; then they grow in size, slow down, and move round the outer part of the torus. The ordinary leapfrogging of  $N = 2$  vortex rings is demonstrated in Fig. 5, which shows two-dimensional cross-sectional slices during a full leapfrogging cycle.

Generalised leapfrogging for  $N = 3$  is shown in Fig. 6. It is apparent that the trajectories of the vortices in the cross-sectional plane are not circular but elliptical. Fig. 7 shows three-dimensional images of the  $N = 3$  vortex bundle during its evolution. This and other three-dimensional images have been prepared using Bob Scharein’s *KnotPlot* software [39].

Generalised leapfrogging of vortex bundles with  $N = 7$  and  $N = 19$  is shown in Fig. 8, 9 and 10. The evolution is qualitatively the same for all values of  $N$ . Fig. 10 shows the cross-section of an  $N = 19$  bundle at different times: clearly the motion of individual vortex lines on the plane is more disordered.

It must be stressed that, after the first reconnection, the meaning of the term leapfrogging is lost: the number of vortex rings may not remain constant, as the constituent vortex rings do not have a well-defined identity any longer.

#### D. Comparison between two-dimensional and three-dimensional leapfrogging

Over 100 years ago, Love [40] showed analytically that two vortex-antivortex pairs (the two-dimensional analogue of two coaxial vortex rings) will perform leapfrogging motion only if the parameter  $\hat{\alpha}$ , defined as the ratio of diameters of the smaller to the larger pair, satisfies the condition  $\hat{\alpha} > 3 - 2\sqrt{2} \approx 0.172 = \hat{\alpha}_c$ . If  $\hat{\alpha} < \hat{\alpha}_c$ , leapfrogging does not occur: the smaller, faster ring 'escapes' the influence of the larger, slower ring and disappears off to infinity. More recently, using numerical methods, Acheson [41] extended Love's work and identified three regimes: (i) when  $\hat{\alpha} < 0.172$  leapfrogging does not occur; (ii) when  $0.172 < \hat{\alpha} < 0.382$  leapfrogging is possible, but is unstable. (iii) when  $\hat{\alpha} > 0.382$ , leapfrogging occurs without instabilities: the system is unaffected by small perturbations.

The comparison of Love's and Acheson's two-dimensional work with our three-dimensional calculation raises the question as to whether there exists a critical  $\hat{\alpha}$  for a system of  $N = 2$  (initially) coplanar, coaxial rings, and, if so, what is its value.

We have performed numerical simulations to identify the range of leapfrogging for  $N = 2$  in our three-dimensional case. We use the criterion that leapfrogging occurs only when  $dR/dt = \dot{R}$  is non-zero: if  $\hat{\alpha}$  is such that  $\dot{R} = 0$  the vortex rings have moved so far apart that one ring has no effect on the other. To make connection to the two-dimensional work of Love and Acheson we relate their parameter  $\hat{\alpha}$  to our  $R/a$ , obtaining

$$\hat{\alpha} = \frac{R - a}{R + a} = \frac{R/a - 1}{R/a + 1}. \quad (7)$$

To determine the range in which  $(R/a)_c$  (hence  $\hat{\alpha}_c$ ) lies, first we proceed by fixing  $R$  and varying  $a$ , then by fixing  $a$  and varying  $R$ , obtaining the same results. We conclude that  $3.5 < (R/a)_c < 3.75$  or, equivalently,  $0.556 < \hat{\alpha}_c < 0.579$ , as opposed to  $\hat{\alpha}_c = 0.172$  in Acheson's and Love's two-dimensional case. Three-dimensional leapfrogging seems more robust than two-dimensional one.

#### E. Turbulent vortex bundles

Table II shows that the  $N = 7$  and  $N = 19$  vortex bundles underwent reconnections before reaching the distance  $\Delta x \approx 10D$  relevant to Borner's experiment, but nevertheless remained coherent and travelled at essentially the same constant speed up to this distance, as shown in Fig. 3. In this section we examine in more detail the long-term evolution of perturbations. We concentrate our attention to the vortex bundle with  $N = 7$  rings (we use slightly different parameters than in Section V A).

Figs. 11 and 12 show side and rear views of what happens at large times; Table III provides a quantitative description, listing, at each selected time, the number of discretization points,  $N_p$ , the number of reconnections which have taken place, the number of rings,  $N$ , left in the bundle, the vortex length,  $\Lambda$ , the average curvature,  $\bar{c}$ , and distance travelled by the centre of vorticity  $\Delta x$  in units of the initial diameter  $D$ .

We find that the vortex rings retain their circular coaxial shapes up to about 57 s when a long-wavelength Kelvin wave starts to grow and eventually causes a vortex reconnection between vortex lines which are almost parallel to each other (in other words, the angle  $\theta$  between the unit tangent vectors  $\mathbf{s} = ds/d\xi$  to the two reconnecting vortex lines is small). Despite the reconnection, the circular symmetry of the vortex configuration is not much altered. An observer tracking the position and velocity of the vortex structure would not notice any change.

In the absence of damping, the short-wavelength perturbations induced by the reconnection cusp travel around the vortex lines which were affected by the reconnection, and induce similar waves on neighboring vortex lines (an effect which we have described in a previous paper [33]). The amount of Kelvin waves is quantified by the average curvature, which grows rapidly. The numerical algorithm has therefore to increase the number of discretization points (as shown in Table III). More reconnections take place, altering the total number of vortex rings in the bundle. At around  $t \approx 70$  s short-wavelength perturbations are visible on the entire vortex bundle, becoming the dominant feature, but still the velocity has not changed significantly yet. Because of the Kelvin waves, the vortex rings are not coplanar any longer, and the vortex length grows significantly.

We know from previous work that large-amplitude Kelvin waves on individual vortex rings slow down the ring's translational motion [42, 43], and a similar effect seems to take place here: when the perturbations are large enough, the vortex bundle slows down significantly. At this late stage of the evolution the vortex bundle has lost most of its symmetry, the number of vortex rings is less than the initial  $N = 7$ , and the structure consists of wiggly, disordered toroidal coils. During the last stage of the evolution, the angle between reconnecting filaments tends to be larger (note Fig. 12(i), where some vortex strands are almost perpendicular to each other), further scrambling the vortex structure.

This scenario seems generic: we find it at other values of parameters and for vortex bundles with a different initial number of rings.

## VI. CONCLUSION

We have computed numerically the evolution of bundles of thin-cored, inviscid vortex filaments, using parameters motivated by the experiments in superfluid helium by Borner and Murakami. We have found that these toroidal vortex structures are relatively robust. They travel at constant speed (which we have modelled in a simple way) and remain coherent for distances which are larger than their own size, confirming the interpretation of the experiments of Borner [1] and Murakami [8]. The individual vortex rings which make up the bundles execute a collective form of leapfrogging motion, moving inside and then outside the other rings, which generalizes the well-known leapfrogging of two vortex rings.

The evolution of these vortex structures is not much affected by the presence of Kelvin waves on individual vortex strands and by vortex reconnections - the translational velocity remains approximately the same. Only when the disturbances are large and these large-scale vortex rings have been reduced to a few disordered toroidal vortex coils the velocity and shape are affected.

Moving away from the parameters of the experiments, we have also found that increasing  $R/a$  leads to increased regularity of the generalised leapfrogging motion, and increased stability of the whole vortex structure.

We hope that these results will stimulate further work on the motion and the coherence of vortex filaments. For example, it would be interesting to investigate the stability of two and three-dimensional bundles analytically, to find whether one should expect stable behaviour for  $t \rightarrow \infty$  (the results which we have presented only refer to length scales and time scales of the experiments).

It would also be interesting to attempt numerical investigations with a very large number of vortex rings keeping the cross-section of the torus constant (this computational may require the use of the vortex tree algorithm [44] recently developed for superfluid turbulence). The natural question is whether the continuous limit of the classical Euler equation is achieved by superposing vortex singularities. For example, one should compare the displacement of vortex lines away from regular trajectories to the distortions of the cross-section of a finite-size core with continuous vorticity distribution found in the context of the Euler equation [45].

## ACKNOWLEDGMENTS

We thank the EPSRC for financial support and Dr A.J. Youd for help with the graphics.

- 
- [1] H. Borner, T. Schmeling and D. Schmidt, Experimental investigation of the circulation of large-scale vortex rings in HeII, *Physica B+C* **108**, 1123-1125 (1981).
  - [2] H. Borner, T. Schmeling and D. Schmidt, Experiments on the circulation and propagation of large-scale vortex rings in HeII, *Phys. Fluids* **26**, 1410-1416 (1983).
  - [3] H. Borner and T. Schmeling, Investigation of large-scale vortex rings in HeII by acoustic measurements of circulation, in *Flow of real fluids*, ed. by G. Meier and F. Obermeier, Lecture Notes in Physics, vol. 235, pp. 135-146, Springer, Berlin/Heidelberg (1985).
  - [4] R. J. Donnelly *Quantized vortices in helium II*, Cambridge U. Press (1991).
  - [5] CF Barenghi and R.J. Donnelly, Vortex rings in classical and quantum systems, *Fluid Dyn. Res.* **41**, 051401 (2009).
  - [6] P.M. Walmsley and A.I. Golov, Quantum and quasi classical types of superfluid turbulence, *Phys. Rev. Letters* **100**, 245301 (2008).
  - [7] G.P. Bewley, and K.R. Sreenivasan, The decay of a quantized vortex ring and the influence of tracer particles, *J. Low Temp. Phys.* **156** 84-94 (2009).

- [8] M. Murakami, M. Hanada, and T. Yamazaki, Visualization study of large-scale vortex rings in HeII. Jap. J. Applied Phys. Suppl. **26**, 107-108 (1987).
- [9] G. Stamm, F. Bielert, W. Fiszdon, and J. Piechna, Counterflow induced macroscopic vortex rings in superfluid helium: visualization and numerical simulation, Physica B **193**, 188-194 (1994).
- [10] G. Stamm, F. Bielert, W. Fiszdon, and J. Piechna, On the existence of counterflow-induced macroscopic vortex rings in he II, Physica B **194-196** 589-590 (1994).
- [11] J. Salort J, et al., Turbulent velocity spectra in superfluid flows, Phys. Fluids **22**, 125102 (2010).
- [12] J. Salort, B. Chabaud, L ev eque E. and P.-E. Roche, Energy cascade and the four-fifths law in superfluid turbulence, Europhys. Lett. **97**, 34006 (2012).
- [13] V. S. L'vov, S. V. Nazarenko, L. Skrbek, Energy Spectra of Developed Turbulence in Helium Superfluids, J. Low Temp. Phys. **145** 125 (2006).
- [14] N. Sasa, T. Kano, M. Machida, V. S. L'vov, O. Rudenko and M. Tsubota, Energy spectra of quantum turbulence: Large-scale simulation and modelling, Phys. Rev. B **84** 054525 (2011).
- [15] C.F. Baggaley, V. L'vov and P.-E. Roche, Turbulent velocity spectra in a quantum fluid: experiments, numerics and models, arXiv:1306.6248v1 (2013).
- [16] W. F. Vinen and J. J. Niemela (2002), Quantum turbulence, J. Low Temp. Phys. **128**, 167 (2002).
- [17] L. Skrebk and K.R. Sreenivasan, Developed quantum turbulence and its decay, Physics of Fluids **24**, 011301 (2012).
- [18] A.W. Baggaley, L.K. Sherwin, C.F. Baggaley, and Y.A. Sergeev, Thermally and mechanically driven quantum turbulence in helium II, Phys. Rev. B **86**, 104501 (2012).
- [19] A.W. Baggaley, C.F. Baggaley, A. Shukurov, and Y.A. Sergeev, Coherent vortex structures in quantum turbulence, Europhys. Lett. **98**, 26002 (2012).
- [20] U. Frisch (1995), *Turbulence. The legacy of A.N. Kolmogorov* (Cambridge University press, Cambridge, UK).
- [21] Y. Oshima, T. Kambe, and S. Asaka, Interaction of two vortex rings moving along a common axis of symmetry, J. Phys. Soc. Japan **38**, 1159-1166 (1975).
- [22] N. Riley and D.P. Stevens, A note on leapfrogging vortex rings, Fluid Dyn. Res. **11**, 235-244 (1991).
- [23] J. Satti and J. Peng, Leapfrogging of two thick-cored vortex rings, Fluid Dyn. Res. **45**, 035503 (2013).
- [24] A.J. Niemi, Exotic statistics of leapfrogging vortex rings, Phys. Rev. Lett. **94**, 124502 (2005).
- [25] In our context, the small difference between hollow core model, solid body uniformly rotating core (Rankine) model, Gross-Pitaevskii core model and actual vortex core in superfluid helium is not significant.
- [26] R.J. Donnelly and C.F. Baggaley, The observed properties of liquid helium at the saturated vapor pressure, J. Phys. Chem. Ref. Data **27**, 1217-1274 (1998).
- [27] P.G. Saffman, *Vortex Dynamics*, Cambridge University Press, Cambridge (1992).
- [28] G.P. Bewley, M.S. Paoletti, K.R. Sreenivasan, and D.P. Lathrop, Characterization of reconnecting vortices in superfluid helium, PNAS **105**, 13707 (2008).
- [29] S. Zuccher, M. Caldari, and C.F. Baggaley, Quantum vortex reconnections, Phys. Fluids **24**, 125108 (2012).
- [30] M. S. Paoletti, M. E. Fisher, and D. P. Lathrop, Reconnection dynamics for quantized vortices, Physica D **239**, 1367-1377 (2010).
- [31] K. W. Schwarz, Three-dimensional vortex dynamics in superfluid <sup>4</sup>He: homogeneous superfluid turbulence, Phys. Lett. B **38** 2398 (1988).
- [32] M. Tsubota & H. Adachi, Simulation of counterflow turbulence by vortex filament, J. Low Temp. Phys. **162** 367-374 (2011).
- [33] A.W. Baggaley and C.F. Baggaley, Spectrum of turbulent Kelvin-waves cascade in superfluid helium, Phys. Rev. B **83**, 134509 (2011).
- [34] A.W. Baggaley and C.F. Baggaley, Vortex-density fluctuations in quantum turbulence, Phys. Rev. B **84** R, 020504 (2011)
- [35] A.W. Baggaley, The sensitivity of the vortex filament method to different reconnection models, J. Low Temp. Physics, **168**, 18 (2012)
- [36] M Leadbeater, T. Winiecki, D.C. Samuels, C.F. Baggaley and C.S. Adams, Sound emission due to superfluid vortex reconnections, Phys. Rev. Lett. **86**, 1410 (2001).
- [37] N. Didden, On the formation of vortex rings: rolling-up and production of circulation, Z. Angew. Math. Phys. **30**, 101-116 (1979).
- [38] K. Shariff and A. Leonard, Vortex rings, Ann. Rev. Fluid Mech. **24**, 235279 (1992).
- [39] Bob Scharein's knot theory computer package *KnotPlot* is available at <http://www.KotPlot.com>.
- [40] A. Love, The motion of paired vortices with a common axis, Proc. Lond. Math. Soc. **25**, 185194 (1894).
- [41] D. Acheson, Instability of vortex leapfrogging, European J. Phys. **21**, 269273 (2000).
- [42] C.F. Baggaley, R. Hanninen, and M. Tsubota, Anomalous translational velocity of vortex ring with finite-amplitude Kelvin waves, Phys. Rev. E **74**, 046303 (2006).
- [43] J.L. Helm, C.F. Baggaley, and A.J. Youd Slowing down of vortex rings in Bose-Einstein condensates Phys. Rev. A **83**, 045601 (2011).
- [44] A.W. Baggaley and C.F. Baggaley, Tree Method for quantum vortex dynamics, J. Low Temp. Physics **166**, 3-20 (2012)
- [45] Y. Fukumoto and Y. Hattori, Curvature instability of a vortex ring, J. Fluid Mech. **526**, 77-115 (2005).



$N$	$\ell$	$R$	$a$	$R/a$
	(cm)	(cm)	(cm)	
1	-	0.06	-	-
2	0.015	0.06	0.0075	8
3	0.015	0.06	0.00866	6.92
7	0.015	0.06	0.015	4
19	0.015	0.12	0.03	4

TABLE I. Initial conditions used in the simulations described in Sect. V A

$N$	Event	$t$	$\Lambda$	$\bar{c}$	$\Delta x/D$	$v$
		(s)	(cm)	$\text{cm}^{-1}$		cm/s
1	start	0	0.377	16.7	0	0.023
	finish	60	0.377	16.7	11.48	0.023
2	start	0	0.754	17.2	0	0.028
	finish	50	0.760	16.7	11.11	0.026
3	start	0	1.131	17.1	0	0.031
	finish	40	1.131	17.2	10.24	0.031
7	start	0	2.639	18.1	0	0.045
	reconnection	26.98	2.712	21.0	9.86	0.040
	finish	30	2.841	69.1	10.91	0.038
19	start	0	14.326	10.9	0	0.047
	reconnection	19.89	14.482	11.9	3.83	0.046
	finish	60	22.451	199.5	10.38	0.028

TABLE II. Outcomes of the simulations described in Sect. V A.

$t$	$N_p$	reconnections	$N$	$\Lambda$	$\bar{c}$	$\Delta x/D$	$v$
(s)				(cm)	(cm <sup>-1</sup> )		(cm/s)
55.875	3528	0	7	3.95	12.1	9.30	0.029
57.75	3528	0	7	3.976	11.9	9.60	0.029
58.5	3593	0	7	3.979	11.8	9.72	0.029
60.0	3747	5	7	4.017	27.0	9.97	0.029
63.75	3714	5	7	4.026	25.8	10.57	0.028
67.5	3925	5	7	4.087	25.7	11.18	0.027
71.25	3944	17	7	4.207	57.3	11.76	0.025
75.0075	4284	34	4	4.327	93.5	12.32	0.024
78.75	4347	47	2	4.516	101.7	12.84	0.023
82.5	4509	68	3	4.68	120.1	13.33	0.021
86.25	4625	86	5	4.847	122.6	13.76	0.018
90.0	4766	102	5	4.976	125.4	14.12	0.015
93.75	4900	124	3	5.105	133.6	14.45	0.014
97.5	4989	142	2	5.213	135.5	14.77	0.013

TABLE III. Development of instabilities for vortex bundle of  $N = 7$  rings, see also Figs. 11 and 12. At each time, the table lists the number of discretization points,  $N_p$ , the number of rings in the bundle,  $N$ , the number of reconnections which have taken place up to that time, the vortex length  $\Lambda$ , the average curvature  $\bar{c}$ , the distance travelled,  $\Delta x$ , in units of the initial diameter,  $D$ , and the velocity  $v$ .



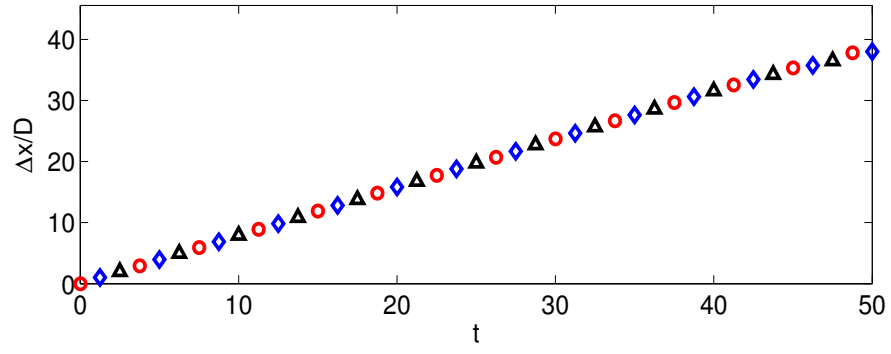


FIG. 2. Ordinary leapfrogging of  $N = 2$  vortex rings. Distance travelled  $\Delta x$  in the x-direction in units of initial diameter  $D = 2R$  vs time  $t$  (s) at  $R = 0.03$  cm,  $a = 0.0075$  cm ( $R/a = 4$ ) for  $\Delta\xi = 0.00149$  cm (red circles),  $\Delta\xi = 0.001$  cm (blue diamonds), and  $\Delta\xi = 0.0005$  cm (black triangle), where the parameter  $\Delta\xi$  determines the spatial numerical resolution. The time step is respectively  $\Delta t = 5 \times 10^{-5}$  s,  $2.5 \times 10^{-5}$  s and  $0.625 \times 10^{-5}$  s.

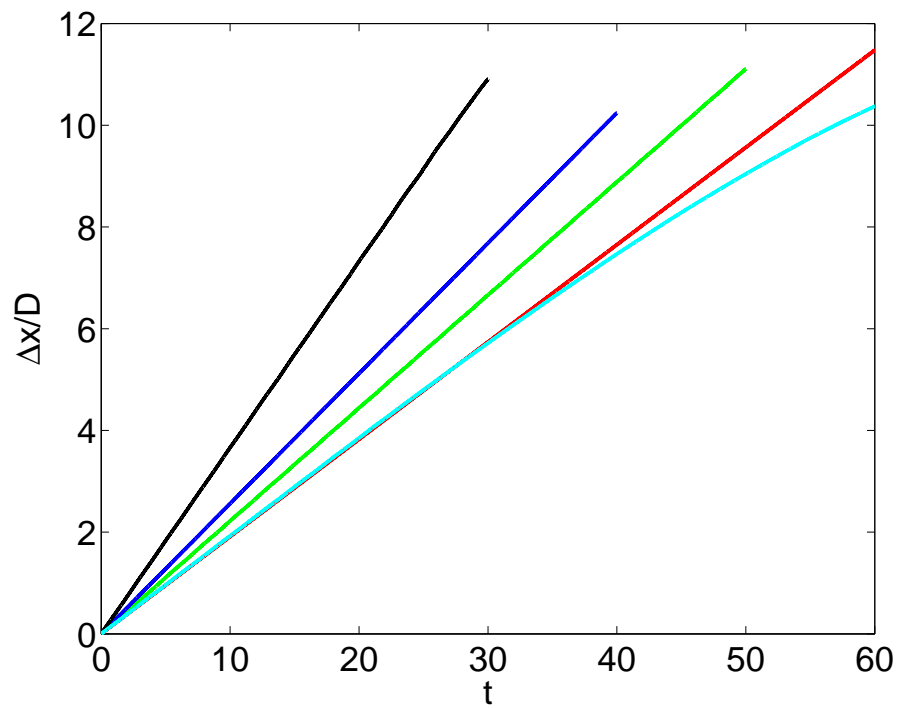


FIG. 3. Distance travelled  $\Delta x$  in units of initial diameter  $D$  vs time  $t$  (s) for vortex bundles consisting of  $N = 1$  (red, fourth curve from left),  $N = 2$  (green, third curve from left),  $N = 3$  (blue, second curve from left),  $N = 7$  (black, first curve at left) and  $N = 19$  (cyan, first curve at right) vortex rings.

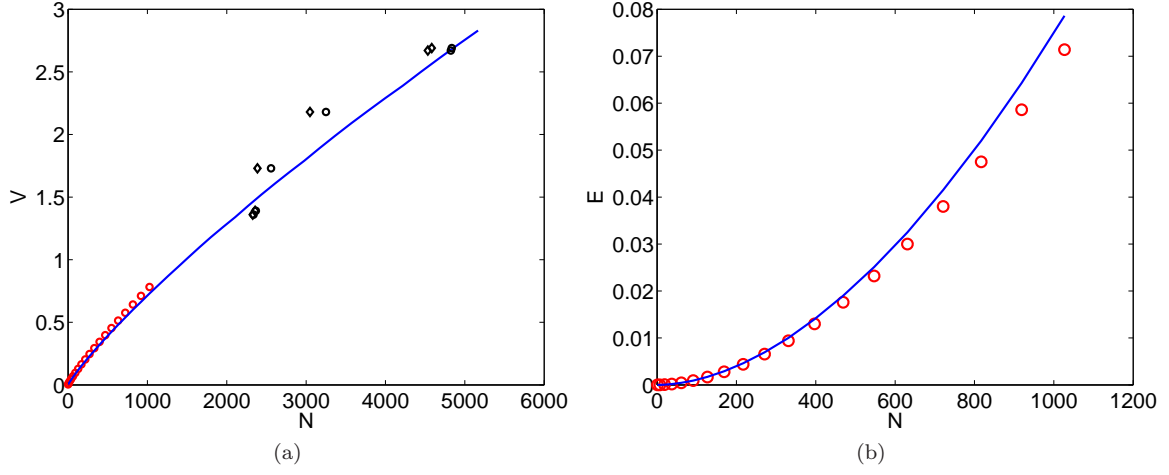


FIG. 4. (a): Translational velocity,  $v$ , and (b): energy,  $E$ , of vortex bundles with  $N$  rings vs number of rings  $N$ . Red circles: numerical simulations for  $N \leq 1027$  (parameters used:  $R = 0.4$  cm,  $\ell = 0.003$  cm,  $a = (n - 1)\ell$  where  $n$  is the number of hexagonal layers in the initial condition,  $\Delta t = 10^{-6}$  s and  $\Delta\xi \approx 0.0335$  cm, corresponding to about 100 discretization points per ring). Black squares and black diamonds: Borner's experimental values at distance  $x = 1.81$  cm and  $x = 4.65$  cm respectively from the orifice. Blue lines: models for velocity  $v'$  and energy  $E'$  from Eq. 5 and 6 respectively.

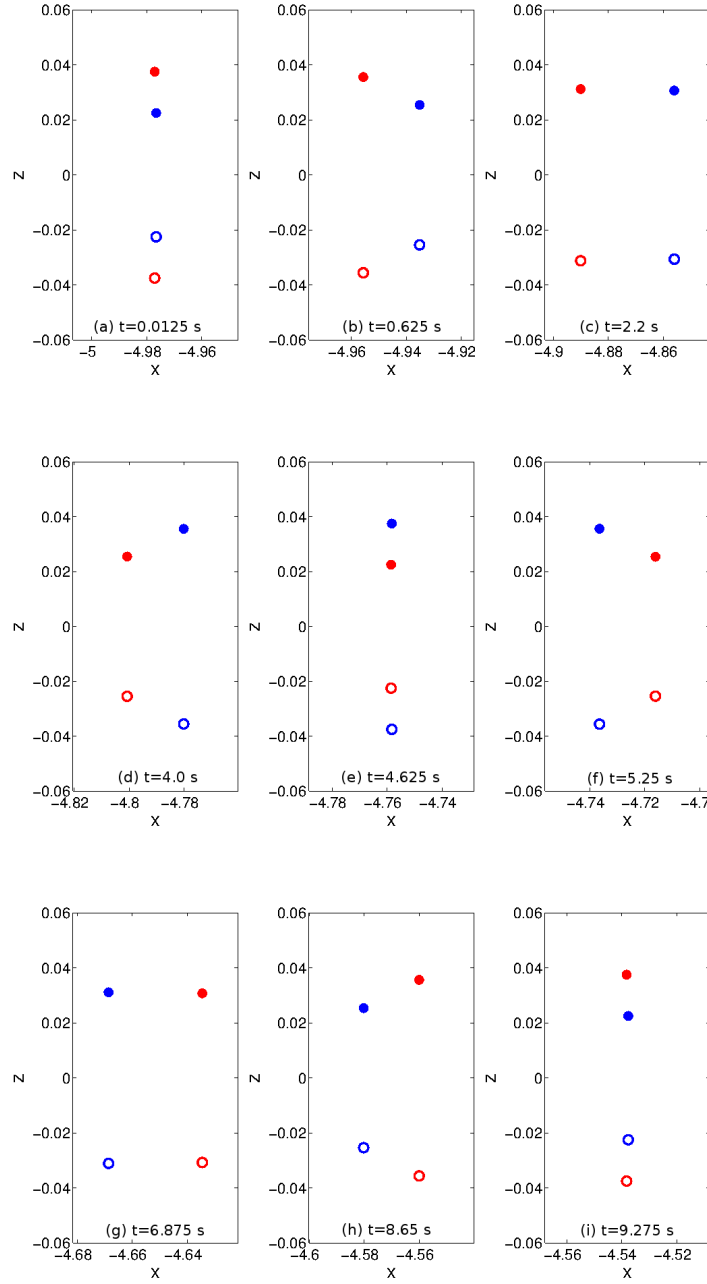


FIG. 5. Ordinary leapfrogging. Cross-sectional slice of vortex bundle for  $N = 2$  at different times. The symbols denote the positions where the vortex rings cut the  $xz$ -plane. The symbols' size is arbitrary. Solid symbols correspond to anticlockwise (positive) circulation, hollow symbols to clockwise (negative) circulation. It is apparent that the motion of the vortex positions on this plane is elliptical. Parameters:  $R = 0.003$  cm,  $a = 0.0075$  cm,  $\ell = 0.015$  cm and  $R/a = 4$ .

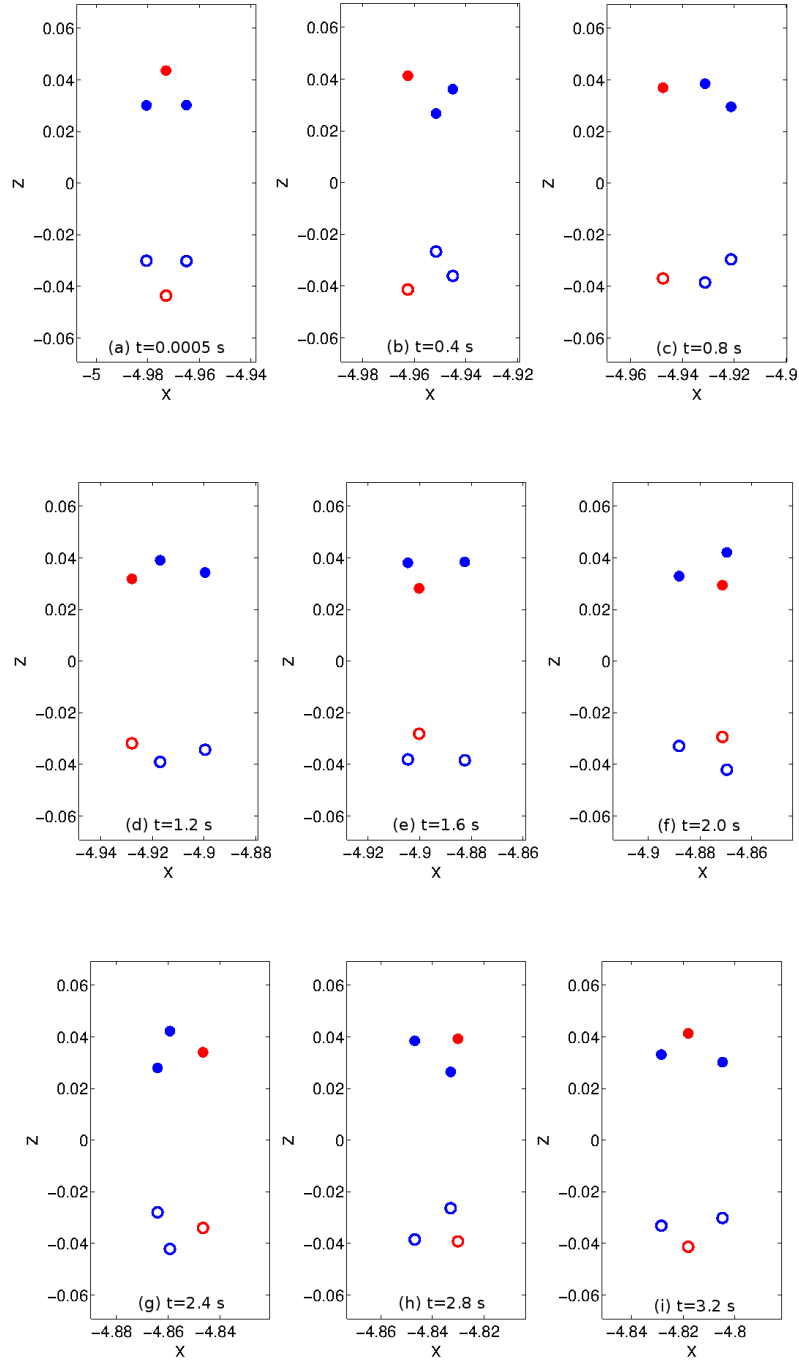


FIG. 6. Generalised leapfrogging. As in Fig. 5, but  $N = 3$ . Note again the ellipticity of the trajectories. One vortex has been marked in red colour to follow its motion. Parameters:  $R = 0.0346$  cm,  $a = 0.00866$  cm,  $\ell = 0.015$  cm and  $R/a = 4$ .



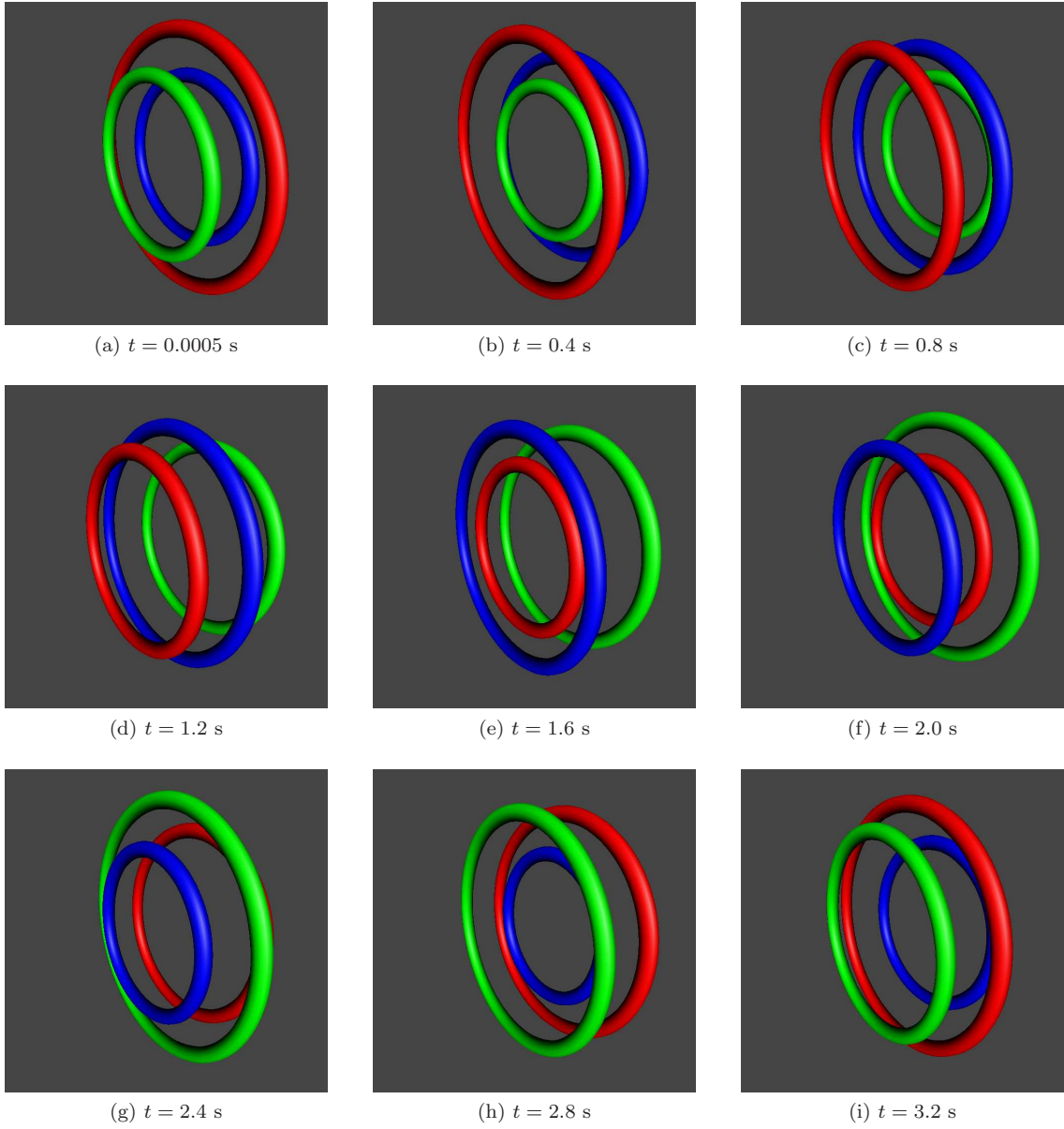


FIG. 7. Generalised leapfrogging. Three-dimensional images of leapfrogging for  $N = 3$  corresponding to the two-dimensional cross-sections of Fig. 6. The colours on different images represent the same vortex ring. For example, notice the red ring on the outside of the torus in (a), which moves around the back of the torus (b), then shrinks (e,f), moves ahead of the other rings (g) and grows in size again (h,i). The arbitrary thickness of the tubes which represent the vortex lines and the size of the box have been adjusted for visualization purpose.

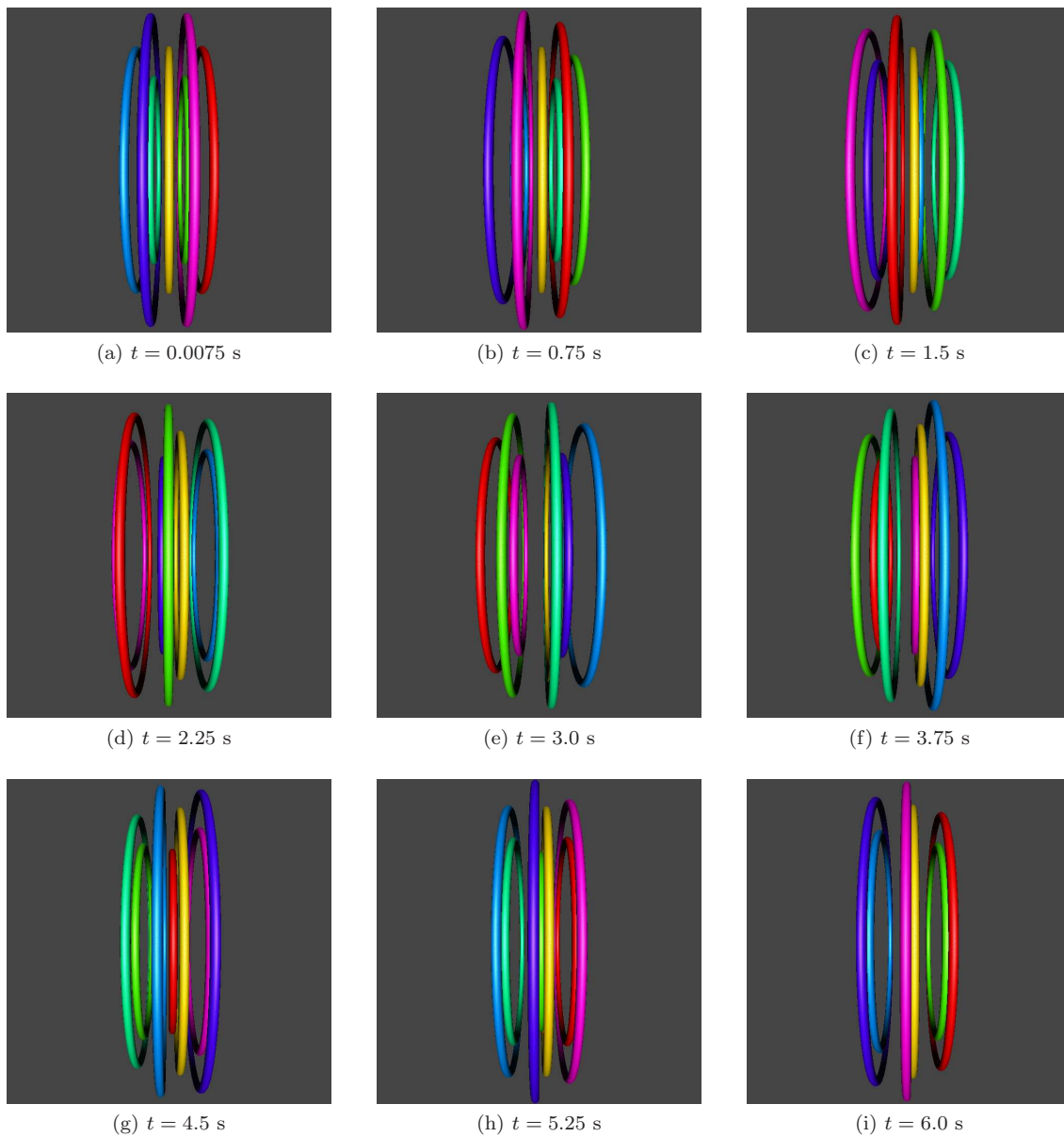


FIG. 8. Generalised leapfrogging. Three-dimensional images of leapfrogging for  $N = 7$ . Again, note how the red ring, initially at the front of the torus (a), moves round to the back (d), then shrinks and overtakes other rings passing inside them (g), and returns to the front (i). Parameters:  $R = 0.0896$  cm,  $a = 0.0223$  cm,  $\ell = 0.0223$  cm and  $R/a = 4$ .

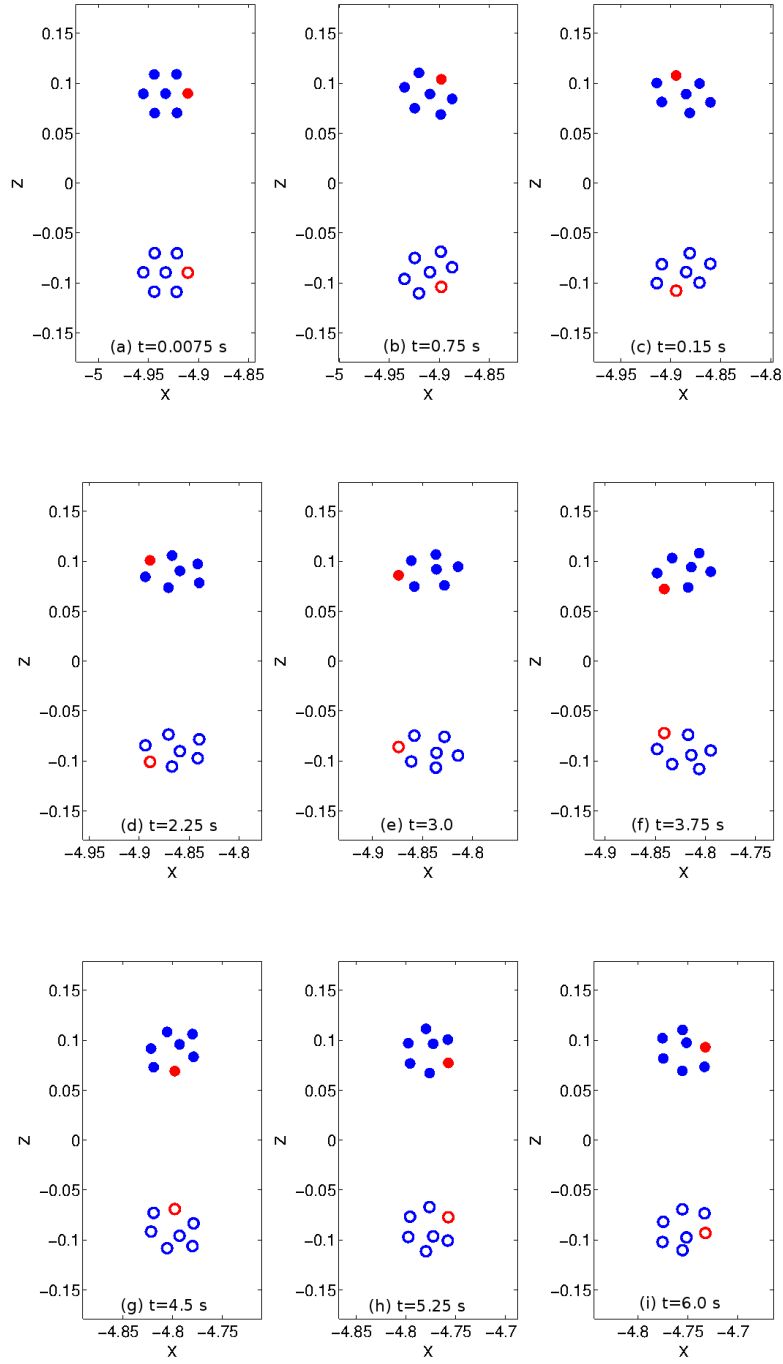


FIG. 9. Generalised leapfrogging. As in Fig. 6, but  $N = 7$ . Note again the ellipticity of the trajectories. One vortex has been marked in red colour to follow its motion.

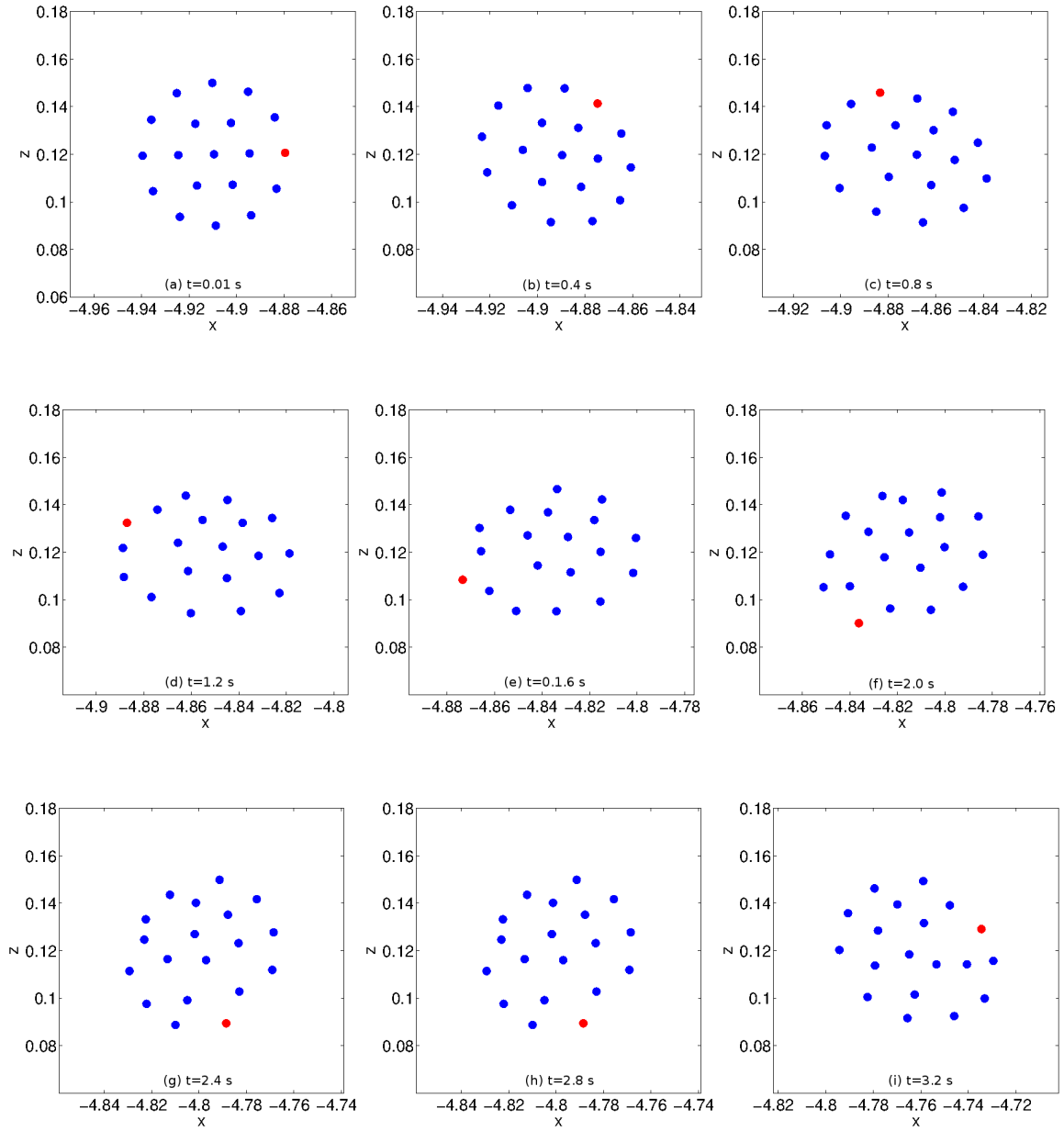


FIG. 10. Generalised leapfrogging. As in Fig. 6, but  $N = 19$ . Only one cross-section is shown. Again, one vortex has been marked in red colour to follow its motion. Parameters:  $R = 0.12$  cm,  $a = 0.03$  cm,  $\ell = 0.015$  cm,  $R/a = 4$ .

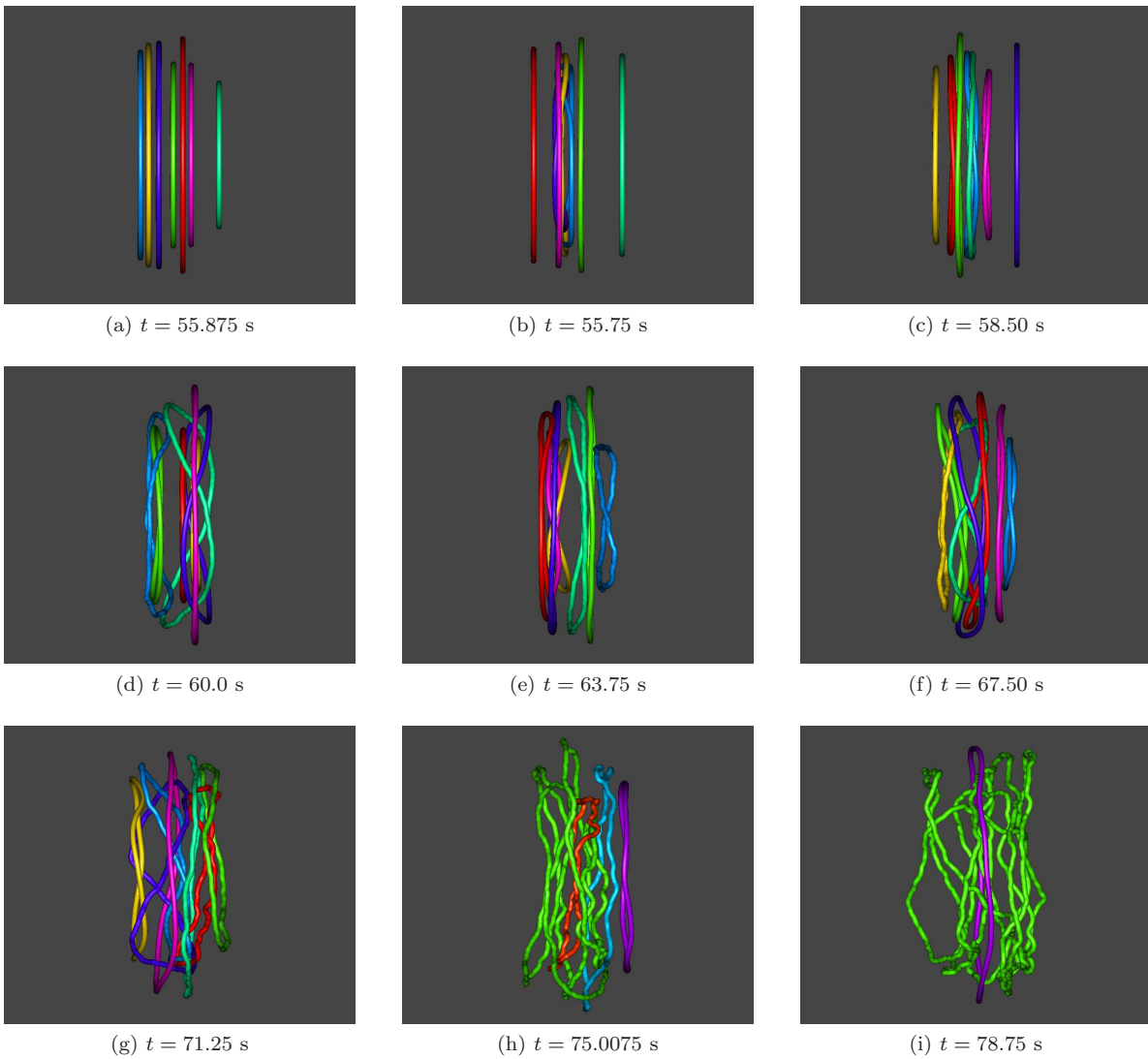


FIG. 11. Development of instabilities on  $N = 7$  vortex bundle, side views at different times (parameters:  $R = 0.0896$  cm,  $a = \ell = 0.0223$  cm,  $R/a = 4$ ,  $\Delta\xi = 0.00149$  cm,  $\ell/\Delta\xi = 15$ ,  $\Delta t = 5 \times 10^{-5}$  s). The rings are coloured arbitrarily (rings of the same colour in any two images are not necessarily the same ring). For the sake of visibility, the scale of the images and the thickness of the vortex lines are also arbitrary.

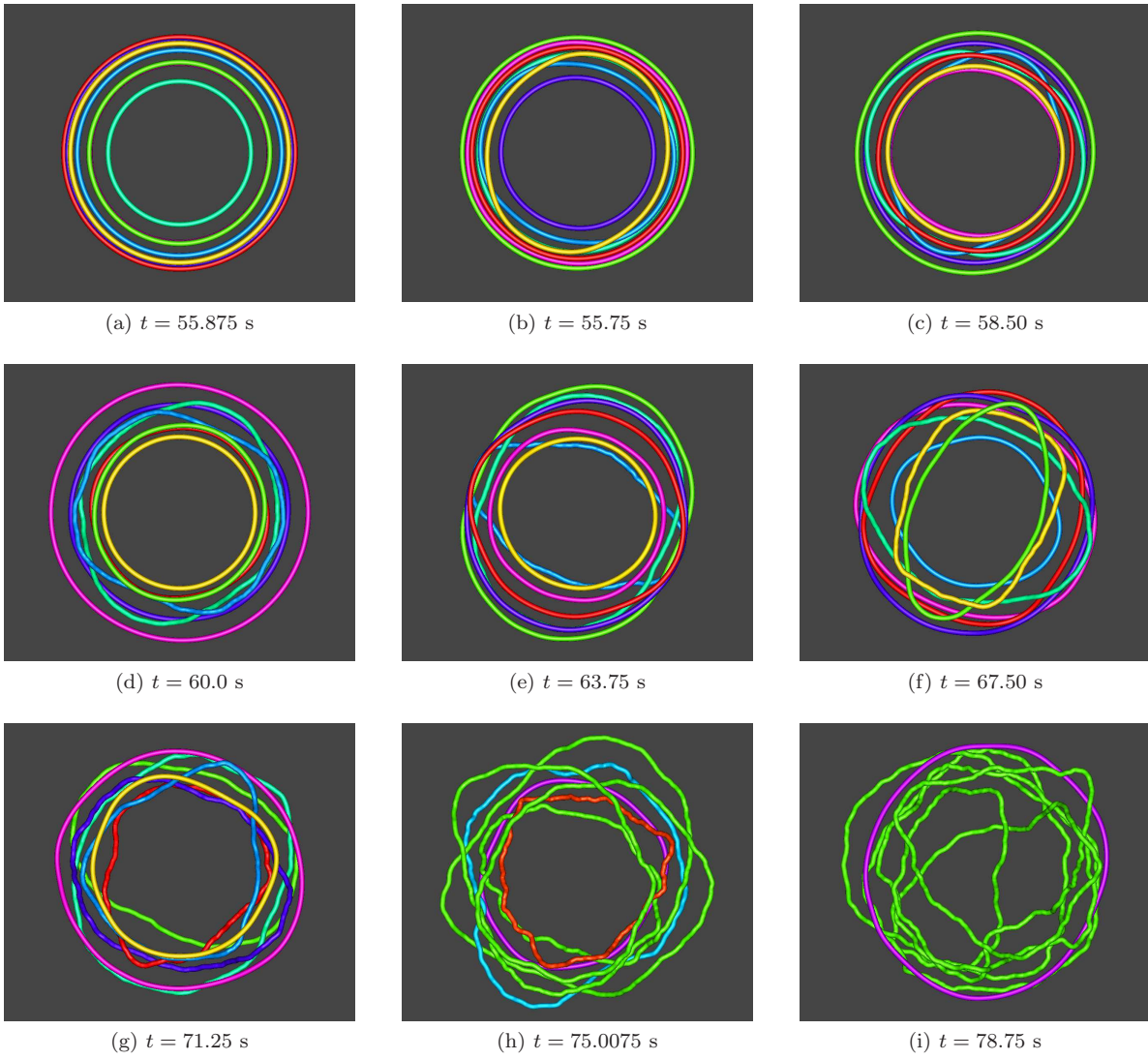


FIG. 12. As in Fig. 11 but rear views.